

# Synthesis and Characterization of Co-Mn Nanocatalyst Prepared by Thermal Decomposition for Fischer-Tropsch Reaction

*Mansouri, Ghobad*

*Department of Chemistry, Payame Noor University, P.O. Box 19395-3697 Tehran, I.R. IRAN*

*Mansouri, Mohsen\*<sup>+</sup>*

*Department of Chemical Engineering, Ilam University, P.O. Box 69315-516 Ilam, I.R. IRAN*

**ABSTRACT:** Nano-structure of Co–Mn spinel oxide was prepared by the thermal decomposition method using  $[\text{Co}(\text{NH}_3)_4\text{CO}_3]\text{MnO}_4$  as the precursor. The properties of the synthesized material were characterized by X-Ray Diffraction (XRD), Brunauer-Emmett-Teller (BET), Transmission Electron Microscopy (TEM), surface area measurements, Energy-Dispersive X-ray (EDX) spectroscopy analysis, UV-Vis spectrophotometer (UV-Vis), Fourier Transform InfraRed (FT-IR), Thermal Gravimetric Analysis (TGA) and Differential Scanning Calorimetry (DSC) analyses. The results show that Co–Mn spinel oxide is spherical in shape and possess crystallite size is about 12 nm. The catalytic activity and product selectivity were also investigated, in a micro-reactor (Fischer–Tropsch Synthesis (FTS) reaction) and the results compared with conventional Co-Mn oxide catalyst. The catalyst performance increased as the particle size of the catalyst decreased. Moreover, the olefin to paraffin ratios was increased, compared to the conventional catalyst.

**KEYWORDS:** Nano-structure catalyst; Co–Mn spinel oxide; Fischer–Tropsch Synthesis.

## INTRODUCTION

Synthesis gas is converted to a complex multicomponent mixture containing linear and branched hydrocarbons and oxygenated products in Fischer–Tropsch Synthesis (FTS) reaction. FTS is an important reaction due to the production of petrochemical feedstocks such as butylenes, propylene, and ethylene from synthesis gas, directly [1-8]. The Fe-Mn and Co-Mn catalysts produce C<sub>2</sub>-C<sub>4</sub> olefins, compared to the (Fe-, or Co-based bimetallic) catalysts [9, 10]. Metallic cobalt

particles dispersed in MnO constitute the Co–Mn catalysts [11], but Fe–Co catalyst favors intermetallic alloy formation [2, 5]. Mn cause to light olefin formation increasing and methane selectivity decreasing [12-14].

Recent studies showed that nano-size metal particles play an essential role to achieve high FTS activity [15-21]. Important technological material is spinel nanocrystal because they have many applications ranging from ultra high magnetic data storage, sorbents, magnetics

---

\* To whom correspondence should be addressed.

+ E-mail: mansouri2010@yahoo.com ; m.mansouri@ilam.ac.ir  
1021-9986/2018/3/1-9 9/\$/5.09

resonance imaging, catalysts, battery materials, biosensing to nanoelectronic material etc [22, 23]. Using of inorganic precursor complexes makes capable materials having well-defined metal loading to be achieved, and synergetic metal-metal or metal-metal oxide interactions which make the better catalytic performance. Many inorganic complexes contain metals in low oxidation states and decomposition enables, pre-reduced, metals to be obtained, facilitating the use of milder catalyst activation conditions that there are other advantages of thermal decomposition of precursor [24-27]. In this paper, we have adopted a simple thermal decomposition of  $[\text{Co}(\text{NH}_3)_4\text{CO}_3]\text{MnO}_4$  precursor method to obtain spinel-type Co-Mn oxide nanocatalyst. This method makes many advantages such as saving energy and time, using cheaply available chemical materials, free organic solvent and easy controlling of reaction temperature. The as-obtained products were characterized by XRD, BET, FT-IR, UV-Vis, TEM, EDX, TGA and DSC.

## EXPERIMENTAL SECTION

### Materials

All the chemical reagents used in our experiments had analytical grade and were used as received without further purification.  $\text{Co}(\text{NO}_3)_2 \cdot 6\text{H}_2\text{O}$ ,  $(\text{NH}_4)_2\text{CO}_3$  and  $\text{KMnO}_4$  were obtained from Merck Company.

### Analysis Method

The weight change of catalyst precursor was analyzed by Thermal Gravimetric Analysis (TGA) and Differential Scanning Calorimetry (DSC) in TGA-PL and DSC-PL England instruments, respectively. Analyses were performed under static air atmosphere at  $10\text{ }^\circ\text{C min}^{-1}$ .

X-Ray Diffraction (XRD) data get from SIEMENS D5000 X-ray diffractometer with  $\text{Cu K}\alpha$  radiation ( $\lambda = 1.54439\text{ \AA}$ ). The spectra were scanned in the range  $2\theta = 5 - 100^\circ$  at a rate of  $2.4^\circ/\text{min}$ . The size of crystallite was accounted using the equation of Scherrer,  $d = 0.9\lambda/(\beta \cos \theta)$ , where  $\lambda$  is the wavelength,  $\beta$  is the Full Width at Half Maximum (FWHM) of the peak and  $\theta$  is the Bragg angle. Infrared spectra were recorded on a Shimadzu system FT-IR 8400S spectrophotometer using KBr pellets. Optical absorption characteristics of nano spinel particles were recorded using a UV-Vis spectrophotometer (Model T80+, PG Instruments, UK).

Transmission Electron Microscopy (TEM) images were obtained on the Philips CM10 to examine the morphology and to directly obtain the particle size of the Co-Mn oxide nanoparticles. First, some calcined precursors were ultrasonically dispersed in ethanol solution, a few drops were put onto a film of porous carbon supported on a copper grid and then dried in air. The average particle size and distribution of particle size were determined by TEM with considering more than 100 particles. Also the elemental composition was determined using the EDS (the energy dispersive X-ray spectroscopy) (IE300X) analysis was performed at several points.

BET surface area was measured using a NOVA 2000 instrument (Quantachrome, USA) using  $\text{N}_2$  adsorption-desorption isotherms at liquid nitrogen temperature ( $-196\text{ }^\circ\text{C}$ ). all the samples (precursor and catalysts) were degassed at  $100\text{ }^\circ\text{C}$  in  $\text{N}_2$  flow for 3h to remove the moisture and other adsorbates. Both the average pore diameter and the pore volume were calculated Barret-Joyner-Halenda (BJH) method from the desorption isotherm [28].

### Preparation of Nano Co-Mn Catalyst

Co-Mn spinel oxide nanocomposite tested in this study were prepared using thermal decomposition procedure which is described in our previous work [29]. A concentrated aqueous  $\text{NH}_3$  (60 mL) was added to a solution of  $(\text{NH}_4)_2\text{CO}_3$  (20 g, 0.21 mol) in 60 ml  $\text{H}_2\text{O}$ , and the mixture was stirred at room temperature for 30 min. To this solution was then added  $\text{Co}(\text{NO}_3)_2 \cdot 6\text{H}_2\text{O}$  (15 g, 0.052 mol) and the resulting solution was stirred at room temperature for 1 h. Then, 8 mL of 30 % hydrogen peroxide was added into the solution dropwise, stirring continuously. The solution poured into a beaker and concentrated using a water bath.  $(\text{NH}_4)_2\text{CO}_3$  (5 g, 0.05 mol) was added slowly during the evaporation time. Then the final solution was filtered and left for slow evaporation in the air until air-stable and water-soluble  $[\text{Co}(\text{NH}_3)_4\text{CO}_3]\text{NO}_3$  red crystals were obtained.  $\text{KMnO}_4$  (7.90 g, 0.05 mol) was added to a solution containing  $[\text{Co}(\text{NH}_3)_4\text{CO}_3]\text{NO}_3$  (12.45 g, 0.05 mol) in 50 ml water and the mixture was stirred for several minutes. The precipitates ( $[\text{Co}(\text{NH}_3)_4\text{CO}_3]\text{MnO}_4$  precursor) were collected by suction filtration, washed with cold water and then air dried (Yield: 82 %).

The  $[\text{Co}(\text{NH}_3)_4\text{CO}_3]\text{MnO}_4$  precursor was calcined at 400 °C in static air in the electric furnace for 1 h. The green-brown powder, Co-Mn oxide was formed and kept in a desiccator.

### Preparation of Conventional Catalyst

For comparative purposes, the Co-Mn conventional catalyst was prepared by co-precipitation method under an air atmosphere. An aqueous solution of  $\text{Co}(\text{NO}_3)_2 \cdot 6\text{H}_2\text{O}$  and  $\text{Mn}(\text{NO}_3)_2 \cdot 6\text{H}_2\text{O}$  (1:1) were pre-mixed, and the resulting solution was stirred and heated to 70 °C in a round-bottomed flask equipped with a condenser. An aqueous solution of  $\text{Na}_2\text{CO}_3$  (0.5 M) was dropwise added to the mixed nitrate solution at 70 °C with stirring until  $\text{pH} = 8 \pm 0.1$  was achieved. The resulting precipitate was filtered and then washed several times with hot distilled water and then dried in an oven at 120 °C for 16 h and subsequently calcined in static air in a furnace at 400 °C for 4 h to obtain the final catalyst.

### Catalyst Testing

Fig. 1 shows a schematic of the experimental setup; the details of the reactor is presented in our previous study [29, 30]. The kind of fixed-bed micro-reactor that made for Fischer–Tropsch synthesis is stainless steel with an inner diameter of 12 mm.

Three mass flow controllers (Brooks Model, 5850E) were utilized to adjust automatically the flow rate of the inlet gases comprising CO,  $\text{H}_2$  and  $\text{N}_2$  (purity of 99.99 %). A mixture of CO,  $\text{H}_2$  and  $\text{N}_2$  was subsequently entered into the reactor, which was placed inside a tubular furnace (Atbin, Model ATU 150-15). Temperature of the reaction was measured and controlled by a thermocouple inserted into the catalytic bed and visually monitored by a computer. To achieve the isothermal conditions in a catalytic bed, the catalyst was diluted with an inert material (quartz). The catalyst was in situ pre-reduced at atmospheric pressure under  $\text{H}_2$ – $\text{N}_2$  flow ( $\text{N}_2/\text{H}_2 = 1$ , flow rate of each gas = 30 ml/min), at 400 °C for 16 h. Experiments were conducted with mixtures of  $\text{H}_2$ , CO, and nitrogen in the 250 °C,  $\text{H}_2/\text{CO}$  feed ratios of 2/1 (mol/mol), the pressure of 7 bar at the gas hourly space velocity (GHSV) 3600  $\text{h}^{-1}$ . The CO conversion percent was calculated according to the normalization method:

CO conversion,

$$\% = \frac{\text{moles CO in} - \text{moles CO out}}{\text{moles CO in}} \times 100 \quad (1)$$

The selectivity percent towards the components was calculated according to:

Selectivity of product  $i$ ,

$$\% = \frac{\text{moles of product } i}{\text{moles CO in} - \text{moles CO out}} \times 100 \quad (2)$$

## RESULTS AND DISCUSSION

### Characterization of Catalyst and its Precursor

The combination of various characterization techniques was used to study the structure and morphology of both precursor and calcined catalysts.

The FT-IR spectra of the  $[\text{Co}(\text{NH}_3)_4\text{CO}_3]\text{MnO}_4$  complex and its decomposition products in 400 °C are shown in Fig. 2. For the complex (Fig. 2a), the peak at 3400  $\text{cm}^{-1}$  should be assigned to  $\text{H}_2\text{O}$  absorbed by the samples or KBr [31].

The additional bands at 3301 and 1621  $\text{cm}^{-1}$  are ascribable to a stretching frequency of the  $\nu(\text{N-H})$  and  $\nu(\text{C=O})$  of the coordinated ligands, respectively. The absorption band at 899  $\text{cm}^{-1}$  is assigned to  $\nu(\text{Mn-O})$  and demonstrates the existence of  $\text{MnO}_4^-$  as counter ion [32]. As shown in Fig. 2b, all the bands associated with the complex clearly disappeared when the complex was decomposed at 400 °C. In Fig. 2b, wide absorption peaks located at around 3421  $\text{cm}^{-1}$  and 1635  $\text{cm}^{-1}$  are caused by the absorbed water molecules and carbon dioxide because the nanocrystalline materials exhibit a high surface-to-volume ratio [33]. The absorption peaks at 535  $\text{cm}^{-1}$  could be ascribed to the stretching vibration of the  $\text{Mn}^{\text{III}}\text{-O}$  in an octahedral environment. The shift of the Mn-O stretching bands to the lower-wave number region in the IR spectrum of the decomposition intermediate shows the decrease in the oxidation number of manganese [34]. The former peak at 642  $\text{cm}^{-1}$  is attributed to the stretching vibration mode of  $\text{Co}^{\text{II}}\text{-O}$  and is tetrahedrally coordinated [35]. These results confirm the Co-Mn spinel structure ( $\text{CoMn}_2\text{O}_4$ ). The XRD results in the next section also support this conclusion.

Optical absorption properties of the  $\text{CoMn}_2\text{O}_4$  nanoparticles were investigated at room temperature by UV–Vis spectroscopy in a phosphoric acid solution (33% W/W). Fig. 3 shows the absorbance spectrum of the  $\text{CoMn}_2\text{O}_4$  sample with two absorption bands in 250 to 350 and

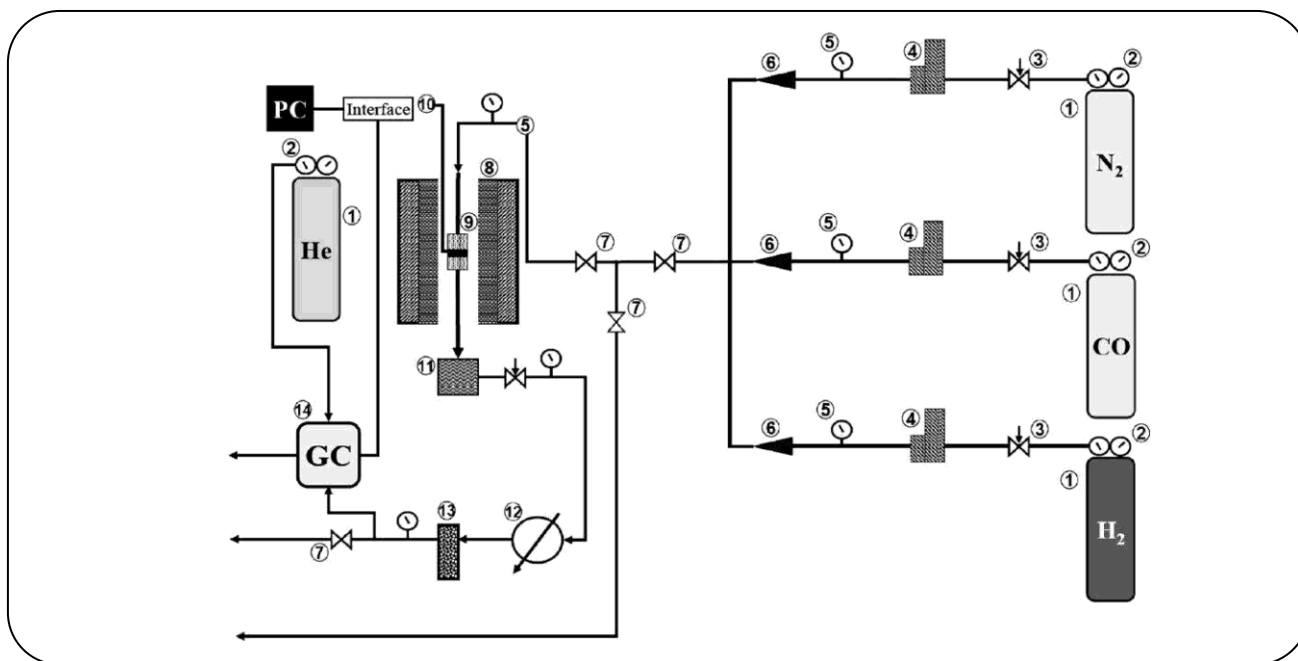


Fig. 1: Schematic representation of the reactor used. (1) Gas cylinders, (2) pressure regulators, (3) needle valves, (4) mass flow controllers, (5) monometers, (6) non-return valves, (7) ball valves, (8) tubular furnace, (9) reactor, (10) catalyst bed, (11) trap, (12) condenser, (13) silica gel column, and (14) gas chromatograph (GC).

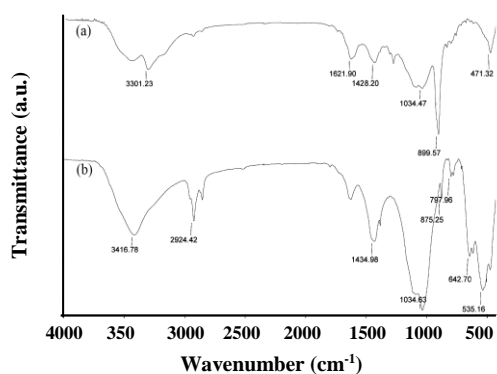


Fig. 2: FT-IR spectrum of (a)  $[\text{Co}(\text{NH}_3)_4\text{CO}_3]\text{MnO}_4$  precursor, and (b) Co-Mn spinel oxide nanoparticles.

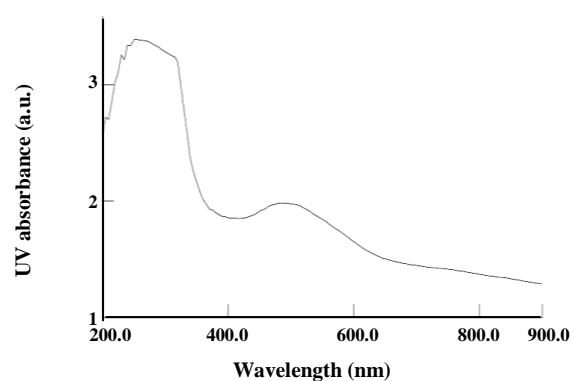


Fig. 3: UV-Visible absorption spectra of  $\text{CoMn}_2\text{O}_4$  nanoparticles.

450 to 650 nm wavelength ranges, which are assigned to the ligand-metal charge transfers. This first band can be assigned to the  $\text{O}^{2-} \rightarrow \text{Co}^{2+}$  and the second one to the  $\text{O}^{2-} \rightarrow \text{Mn}^{3+}$  charge transfers. Compared with the absorptions bands for nanocubes reported by Zeng *et al.*, [36] the corresponding absorptions are blue shifted. The significant blue-shift is caused mainly by the quantum size effect of nanocrystals.

Fig. 4 shows the XRD results of the precursor prepared by the thermal decomposition method. The diffraction lines at  $2\theta = 15.8, 19.4, 23.5, 26.7, 28$  and

$29.9^\circ$  are of high intensity and of low half-width, which are typical of a well-crystallized sample. No obvious peaks of impurities were seen in this pattern. The XRD pattern for the calcined prepared from the  $[\text{Co}(\text{NH}_3)_4\text{CO}_3]\text{MnO}_4$  precursor and the conventional catalyst are presented in Fig. 5. As can be seen, all diffraction peaks related to  $[\text{Co}(\text{NH}_3)_4\text{CO}_3]\text{MnO}_4$  disappeared at  $400^\circ\text{C}$  and new broad peaks appeared. The broadening of the peaks demonstrates the nanometric character of the particles.

The XRD pattern of the calcined  $[\text{Co}(\text{NH}_3)_4\text{CO}_3]\text{MnO}_4$  precursor when compared with JCPDS: 77-0471 reveals

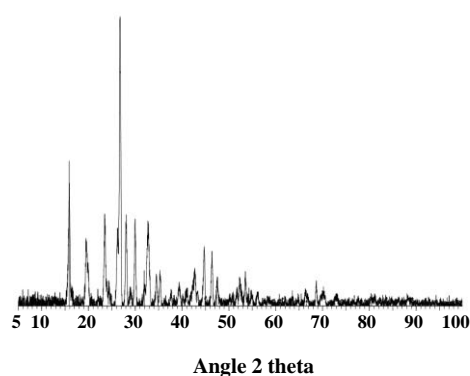


Fig. 4: X-ray diffraction pattern of  $[\text{Co}(\text{NH}_3)_4\text{CO}_3]\text{MnO}_4$  precursor.

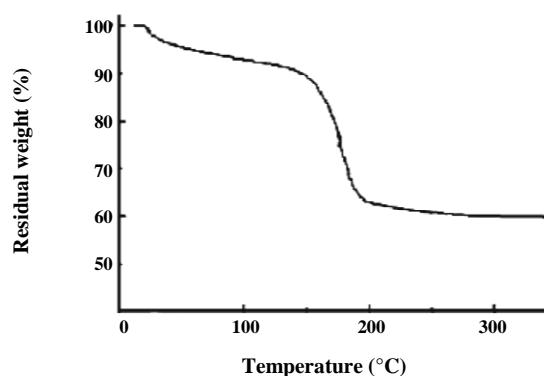


Fig. 6: TGA curves of  $[\text{Co}(\text{NH}_3)_4\text{CO}_3]\text{MnO}_4$  precursor.

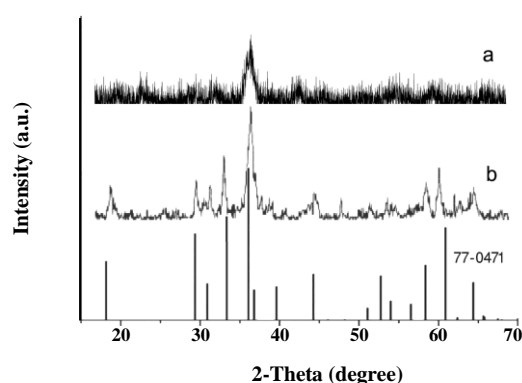


Fig. 5: X-ray diffraction pattern of (a) calcined  $[\text{Co}(\text{NH}_3)_4\text{CO}_3]\text{MnO}_4$  precursor and (b) conventional catalyst.

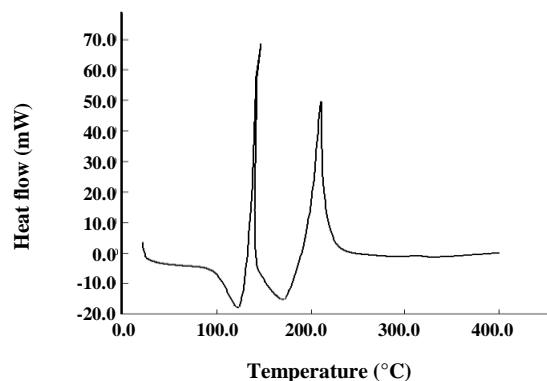


Fig. 7: DSC curve for  $[\text{Co}(\text{NH}_3)_4\text{CO}_3]\text{MnO}_4$  precursor.

the structure as spinel oxide ( $\text{CoMn}_2\text{O}_4$ ). No peaks from any other phases of Co-Mn oxide were observed. The characteristic peak at  $2\theta = 37^\circ$  corresponds to the Co-Mn oxide was used to calculate the crystallite size. The average crystallite size prepared with calcined  $[\text{Co}(\text{NH}_3)_4\text{CO}_3]\text{MnO}_4$  precursor and conventional catalysts were estimated to be about 12.2 and 23.4 nm, respectively, by the Scherrer formula.

The TGA data for the  $[\text{Co}(\text{NH}_3)_4\text{CO}_3]\text{MnO}_4$  shows two steps for weight loss (Fig. 6). It is clearly visible that the first weight loss occurred below 130 °C, corresponding to the expulsion of physisorbed water and the removal of crystallization water.

The second stage (150–210 °C) is due to the decomposition of  $[\text{Co}(\text{NH}_3)_4\text{CO}_3]\text{MnO}_4$  to cobalt and manganese oxides phases that were identified by XRD technique. Almost no weight loss was observed above 250 °C, implying the presence of only Co-Mn spinel oxide

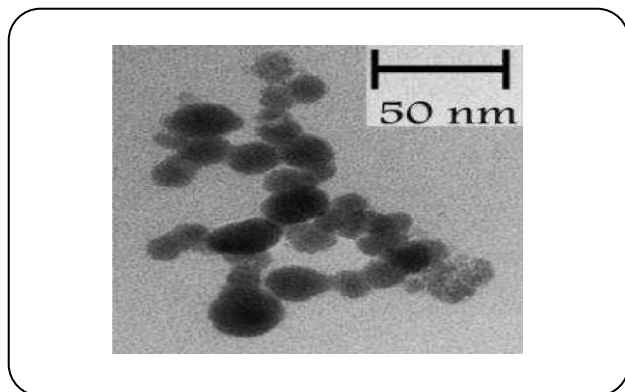
in this temperature range. In order to provide further evidence for the presence of the various species and evaluates their thermal behavior, DSC measurement was performed. DSC curve for the  $[\text{Co}(\text{NH}_3)_4\text{CO}_3]\text{MnO}_4$  precursor exhibits one endothermic peak and two exo-effects (Fig. 7).

The endothermic peak between 80 and 130 °C is assigned to the evaporation and volatilization of residue free water. Two exothermic peaks in the region 130–250 °C are attributed to the decomposition of  $[\text{Co}(\text{NH}_3)_4\text{CO}_3]\text{MnO}_4$  to Co-Mn spinel oxide.

A TEM image of Co-Mn spinel oxide nanoparticle prepared by thermal decomposition of  $[\text{Co}(\text{NH}_3)_4\text{CO}_3]\text{MnO}_4$  was illustrated in Fig.8. It can be seen that the nanoparticles could be dispersed very well in ethanol, a few aggregates could be found and the average particle size is about 12 nm. The average size of particles determined by TEM analysis suggests

**Table 1: Textural of the precursor, nano and conventional catalysts.**

Sample	BET surface area, m <sup>2</sup> /g	Pore volume, cm <sup>3</sup> /g	Average pore diameter, nm
[Co(NH <sub>3</sub> ) <sub>4</sub> CO <sub>3</sub> ]MnO <sub>4</sub>	11.32	0.12	16.89
Nano catalyst	74.28	0.21	13.32
Conventional catalyst	46.59	0.18	13.41

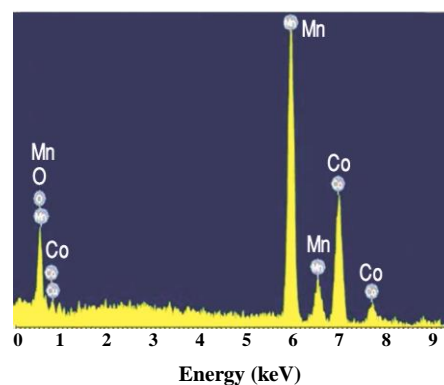
**Fig. 8: TEM micrograph of Co–Mn spinel oxide nanoparticles.**

that the obtained nanoparticles might be monocrystalline i.e. the average particle size determined by TEM is consistent with the average crystallite size determined by XRD.

The EDX analysis (energy-dispersive X-ray spectroscopy) of the fresh calcined catalyst refers to the presence of O, Mn and CO (Fig. 9), which shows to be true that this material is comprised of oxidic phases of cobalt and manganese. This is supported by the X-ray diffraction data, which showed the existence of oxide phases of cobalt and manganese. BET surface area, pore volume and pore diameter of the precursor ([Co(NH<sub>3</sub>)<sub>4</sub>CO<sub>3</sub>]MnO<sub>4</sub>), and conventional catalysts are summarized in Table 1.

As shown in Table 1, the BET surface area and pore volume of the precursor are very low, about 11.32 m<sup>2</sup>/g and 0.12 cm<sup>3</sup>/g, respectively. After calculations, it can be seen that the BET surface area and pore volume increased to 74.28 m<sup>2</sup>/g and 0.21 cm<sup>3</sup>/g, respectively. By comparing the BET surface areas, the nanocatalysts prepared by thermal decomposition of [Co(NH<sub>3</sub>)<sub>4</sub>CO<sub>3</sub>]MnO<sub>4</sub> has higher BET surface area than conventional catalyst. It can be attributed to the adopted preparation method.

Also, it could be seen that the average pore diameter for the used samples showed a little difference. To calculate the pore sizes, the BJH method was applied [28]. There exist a number of other techniques to determine

**Fig. 9: EDX-spectra of Co–Mn spinel oxide nanoparticles.**

the pore size characteristics which are based on different assumptions and pore geometry. Thus, specific values depend on the method, but the general findings are expected to be valid independent of any standard method employed.

#### *Effect of Catalyst Crystal Size*

Table 2 displays the effect of the catalyst crystal size on catalyst activity, product selectivity and hydrocarbons distribution with different space velocity at the same time on stream. It is showed that the CO conversion was increased when the crystal size of the catalyst from conventional to nanostructure catalyst decrease. The methane selectivity was decreased and the C<sub>2</sub>–C<sub>4</sub> light olefins selectivity was increased at the same time in comparison with the conventional catalyst. Selectivity towards higher hydrocarbons shows an increasing trend in carbon number from nano to conventional catalyst. Primary products of the FTS reaction over the cobalt-manganese based catalyst and may undergo to paraffin by hydrogenation as a secondary reaction are 1-Alkenes [11]. The olefin/paraffin ratio is a base ratio to demonstrate the presence of the secondary reactions in total FT synthesis [37]. The results presented in Table 2. show that the olefin/paraffin ratios are increased from conventional to nanocatalyst.

Table 2: Catalyst activity and product selectivity<sup>a</sup>.

Catalyst	Average crystallite size (nm)	CO conv <sup>b</sup>	Selectivity <sup>c</sup>			Olefin/Paraffin
			CH <sub>4</sub>	Olefin (C <sub>2</sub> -C <sub>4</sub> )	C <sub>5+</sub>	
Conventional Catalyst	23.4	9.64	23.94	26.85	21.76	1.09
Nano Catalyst	12.2	15	18.45	30.01	20.95	1.22

a) reaction conditions: 250 °C, 7 bar, H<sub>2</sub>/CO = 2, space velocity = 3600 h<sup>-1</sup>. Time on stream is 70 h.

b) percentage CO conversion.

c) selectivity based on carbon moles.

## CONCLUSIONS

In order to make use of Co–Mn oxide catalyst, spinel-type Co–Mn oxide nanoparticles were prepared by the thermal decomposition method using [Co(NH<sub>3</sub>)<sub>4</sub>CO<sub>3</sub>]MnO<sub>4</sub> as the precursor. It was a simple and suitable way for the preparation of binary catalysts for different catalytic processes. The XRD pattern (Scherrer equation) and TEM images indicated that the average nanocrystallite size of Co–Mn spinel oxide was about 12 nm. Catalytic activity and product selectivity were conducted in a fixed-bed stainless steel reactor and compared with conventional cobalt - manganese catalyst. The results showed that the BET surface area and pore volume were increased with decreasing the crystal size of the catalyst from conventional to nanocatalyst. The two catalysts' performance comparison shows that the nanocatalyst has higher selectivity to C<sub>2</sub>-C<sub>4</sub> light olefin, higher activity, lower selectivity to CH<sub>4</sub> and C<sub>5+</sub> hydrocarbons after 70 h time on stream.

Received: Jan. 1, 2017 ; Accepted: Sep. 25, 2017

## REFERENCES

- [1] Tihay F., Pourroy G., Richard-Plouet M., Roger A.C., Kiennemann A., [Effect of Fischer–Tropsch Synthesis on the Microstructure of Fe–Co-Based Metal/Spinel Composite Materials](#), *Appl. Catal. A Gen.*, **206**: 29-42 (2001)
- [2] Duvenhage D.J., Coville N., [Fe:CoTiO<sub>2</sub> Bimetallic Catalysts for the Fischer-Tropsch Reaction I. Characterization and Reactor Studies](#), *J. Appl. Catal. A Gen.* **153**: 43-67 (1997)
- [3] Cabet C., Roger A.C., Kiennemann A., Läkamp S., Pourroy G., [Synthesis of New Fe–Co Based Metal/Oxide Composite Materials: Application to the Fischer–Tropsch Synthesis](#), *J. Catal.*, **173**: 64-73 (1998)
- [4] Gholami Z., Zabidi N.A.M., Gholami F., [Synthesis and Characterization of Niobium-Promoted Cobalt/Iron Catalysts Supported on Carbon Nanotubes for the Hydrogenation of Carbon Monoxide](#), *J. Fuel Chem. Technol.*, **44**: 815–821 (2016)
- [5] Tihay F., Roger A.C., Kiennemann A., Pourroy G., [Fe–Co Based Metal/Spinel to Produce Light Olefins from Syngas](#), *Catal. Today*, **58**: 263-269 (2000)
- [6] Reshetenko T.V., Avdeeva L.B., Khassin A.A., Kustova G.N., Ushakov V.A., Moroz E.M., Shmakov A.N., [Coprecipitated Iron-Containing Catalysts \(Fe-Al<sub>2</sub>O<sub>3</sub>, Fe-Co-Al<sub>2</sub>O<sub>3</sub>, Fe-Ni-Al<sub>2</sub>O<sub>3</sub>\) for Methane Decomposition at Moderate Temperatures: I. Genesis of Calcined and Reduced Catalysts](#), *Appl. Catal. A Gen.*, **268**: 127-138 (2004)
- [7] de la Pen'a O'Shea V.A., Menéndez N.N., Tornero J.D., Fierro J.L.G., [Unusually High Selectivity to C<sub>2</sub><sup>+</sup> Alcohols on Bimetallic CoFe Catalysts During CO Hydrogenation](#), *Catal. Lett.*, **88**: 123-128 (2003)
- [8] Mirzaei A.A., Habibpour R., Kashi E., [Preparation and Optimization of Mixed Iron Cobalt Oxide Catalysts for Conversion of Synthesis Gas to Light Olefins](#), *Appl. Catal. A Gen.*, **296**: 222-231 (2005).
- [9] van der Laan G.P., Beenackers A.A.C.M., [Kinetics and Selectivity of the Fischer-Tropsch Synthesis: A Literature Review](#), *Catal. Rev. Sci. Eng.*, **41**: 255-318 (1999)
- [10] González-Cortés S.L., Rodulfo-Baechler S.M.A., Oliveros A., Orozco J., Fontal B., Mora A.J., Delgado G., [Synthesis of Light Alkenes on Manganese Promoted Iron and Iron-Cobalt Fischer-Tropsch Catalysts](#), *React. Kinet. Catal. Lett.*, **75**: 3-12 (2002).
- [11] Keyser M.J., Everson R.C., Espinoza R.L., [Fischer–Tropsch Studies with Cobalt–Manganese Oxide Catalysts: Synthesis Performance in a Fixed bed Reactor](#), *Appl. Catal. A Gen.*, **171**: 99-107 (1998).

- [12] Barrault J., Selective Hydrogenation of Carbon Monoxide on Supported Iron or Cobalt Catalysts. Effects of Manganese Oxide and (or) Chlorine, *Stud. Surf. Sci. Catal.*, **11**: 225-231 (1982)
- [13] Barrault J., Forquy C., Menezo J.C., Maurel R., Selective Hydrocondensation of CO to Light Olefins with Alumina-Supported Iron Catalysts, *React. Kinet. Catal. Lett.*, **15**: 153-158 (1980).
- [14] Barrault J., Forquy C., Perrichon V., Effects of Manganese Oxide and Sulphate on Olefin Selectivity of Iron Supported Catalysts in the Fischer-Tropsch Reaction, *Appl. Catal.*, **5**: 119-125 (1983).
- [15] Mansouri M., Atashi H., Fischer-Tropsch Synthesis over Potassium-Promoted Co-Fe/SiO<sub>2</sub> Catalyst, *Indian J. Chem. Tech.*, **23**: 453-461 (2016)
- [16] Feyzi M., Hassankhani A., TiO<sub>2</sub> Supported Cobalt-Manganese Nano Catalysts for Light Olefins Production from Syngas, *J. Energy Chem.*, **22**: 645-652 (2013).
- [17] Park J.Y., Lee Y.J., Karandikar P.R., Jun K.W., Ha K.S., Park H.G., Fischer-Tropsch Catalysts Deposited with Size-Controlled Co<sub>3</sub>O<sub>4</sub> Nanocrystals: Effect of Co Particle Size on Catalytic Activity and Stability, *Appl. Catal. A Gen.*, **411-412**: 15-23 (2012).
- [18] Zeng B., Hou B., Jia L., Li D., Sun Y., Fischer-Tropsch Synthesis over Different Structured Catalysts: The Effect of Silica Coating onto Nanoparticles, *J. Mol. Catal. A Chem.*, **379**: 263-268 (2013).
- [19] Nakhaei Pour A., Housaindokht M.R., Torabi F., Water-Gas Shift Kinetics over Lanthanum-Promoted Iron Catalyst in Fischer-Tropsch Synthesis: Thermodynamic Analysis of Nanoparticle Size Effect, *J. Iran Chem. Soc.*, **11**: 1639-1648 (2014).
- [20] Li T., Wang H., Yang Y., Xiang H., Li Y., Study on an Iron-Nickel bimetallic Fischer-Tropsch Synthesis Catalyst, *Fuel Process. Tech.*, **118**: 117-124 (2014)
- [21] Farzad S., Haghtalab A., Rashidi A., Comprehensive Study of Nanostructured Supports with High Surface Area for Fischer-Tropsch Synthesis, *J. Energy Chem.*, **22**: 573-581 (2013).
- [22] Zhang H.T., Chen X.H., Size-Dependent X-Ray Photoelectron Spectroscopy and Complex Magnetic Properties of CoMn<sub>2</sub>O<sub>4</sub> Spinel Nanocrystals, *Nanotechnology*, **17**: 1384-1390 (2006)
- [23] He T., Chen D., Jiao X., Wang Y., Duan Y., Solubility-Controlled Synthesis of High-Quality Co<sub>3</sub>O<sub>4</sub> Nanocrystals, *Chem. Mater.*, **17**: 4023-4030 (2005).
- [24] Tavakoli H., Mamoozy R.S., Zarei A.R., Inverse Co-Precipitation Synthesis of Copper Chromite Nanoparticles, *Iran. J. Chem. Chem. Eng. (IJCCE)*, **35**: 51-55 (2016).
- [25] Ahmadi S.H., Davar P., Manbohi A., Adsorptive Removal of Reactive Orange 122 from Aqueous Solutions by Ionic Liquid Coated Fe<sub>3</sub>O<sub>4</sub> Magnetic Nanoparticles as an Efficient Adsorbent, *Iran. J. Chem. Chem. Eng. (IJCCE)*, **35**: 63-73 (2016).
- [26] Li D., Zhong G-Q., Zang Q., Solid-Solid Synthesis, Crystal Structure and Thermal Decomposition of Copper(II) Complex of 2-Picolinic Acid, *Iran. J. Chem. Chem. Eng. (IJCCE)*, **35**: 21-29 (2016).
- [27] Rad A.R.S., Khoshgouei M.B., Rezvani A.R., Water Gas Shift Reaction over Zn-Ni/SiO<sub>2</sub> Catalyst Prepared from Zn(H<sub>2</sub>O)<sub>6</sub>]2[Ni(NCS)<sub>6</sub>].H<sub>2</sub>O/SiO<sub>2</sub> Precursor, *J. Mol. Catal. A Chem.*, **344**: 11-17 (2011)
- [28] Barrett E.P., Joyner L.G., Halenda P.P., The Determination of Pore Volume and Area Distributions in Porous Substances. I. Computations from Nitrogen Isotherms, *J. Am. Chem. Soc.*, **73**: 373-380 (1951)
- [29] Mansouri M., Atashi H., Farshchi Tabrizi F., Mirzaei A.A., Mansouri G., Kinetics Studies of Nano-Structured Cobalt-Manganese Oxide Catalysts in Fischer-Tropsch Synthesis, *J. Ind. Eng. Chem.*, **19**: 1177-1183 (2013)
- [30] Mansouri, M. Atashi, H. Khalilipour, M.M. Setaresheenas, N. Shahraki, F., Rate Expression of Fischer-Tropsch Synthesis Over Co-Mn Nanocatalyst by Response Surface Methodology (RSM), *J. Korean Chem. Soc.*, **57**: 769-777 (2013).
- [31] Kaviyarasu K., Raja A., Devarajan P.A., Structural Elucidation and Spectral Characterizations of Co<sub>3</sub>O<sub>4</sub> Nanoflakes, *Spectrochim. Acta. A Mol. Biomol. Spectrosc.*, **114**: 586-591 (2013)
- [32] Kótai L., Argay G., Holly S., Szentmihályi K., Keszler Á., Pukánszky B., Anorg Z., Study on the Existence of Hydrogen Bonds in Ammonium Permanganate, *Z. Anorg. Allg. Chem.*, **627**: 114-118 (2001).
- [33] Zhang Y.C., Qiao T., Hu X.Y., Hu X.Y., Zhou W.D., Simple Hydrothermal Preparation of  $\gamma$ -MnOOH Nanowires and Their Low-Temperature Thermal Conversion to  $\beta$ -MnO<sub>2</sub> Nanowires, *J. Cryst. Growth.*, **280**: 652-657 (2005).

- [34] Rohani Bastami T., Entezari M.H., [A Novel Approach for the Synthesis of Superparamagnetic Mn<sub>3</sub>O<sub>4</sub> Nanocrystals by Ultrasonic Bath](#), *Ultrason. Sonochem.*, **19**: 560-569 (2012).
- [35] Salavati-Niasari M., Khansari A., Davar F., [Synthesis and Characterization of Cobalt Oxide Nanoparticles by Thermal Treatment Process](#), *Inorg. Chim. Acta.*, **362**: 4937-4942 (2009).
- [36] Xu R., Zeng H.C., [Synthesis of Co<sub>3</sub>O<sub>4</sub> Nanocubes and Their Close- and Non-Close-Packed Organizations](#), *Langmuir*, **20**: 9780-9790 (2004).
- [37] Dry M.E., In [“The Fischer–Tropsch Synthesis, Catalysis: Science and Technology”](#), Anderson J.R., Boudart M., (eds.) (Springer-Verlag: NY) pp.160-255 (1981).